FREQUENCY-DEPENDENT VISCOELASTIC TIDES OF MERCURY. A. Stark[1], H. Hussmann[1], A. Fienga[2,3], X. Hu[4], J. Oberst[4], N. Rambaux[3], D. Baguet[3], A. Memin[2], A. Briaud[2]. [1]Deutsches Zentrum für Luft- und Raumfahrt (DLR), Berlin, Germany, [2]Geoazur, CNRS, Observatoire de la Cote d'Azur, Universite Cote d'Azur, Valbonne, France, [3]IMCCE, Observatoire de Paris, PSL University, CNRS, Sorbonne Universite, Paris, France, [4]Institute of Geodesy and Geoinformation Science, Technische Universität Berlin, Berlin, Germany.

Introduction: The planet Mercury is closest to the Sun and undergoes significant tidal deformation due to tides raised by the Sun. Mercury's large eccentricity and its 3:2 spin-orbit resonance lead to a deformation pattern not found elsewhere in the Solar System. In fact, the tidal potential would not vanish even when Mercury's orbit would be perfectly circular, in contrast to, e.g., icy moons or Earth's moon. The amplitude and the phase of the tidal deformation reveals crucial information about the interior structure and rheology of Mercury. While Mercury's elastic response to tides was already observed using the Mercury Surface, Space Environment, Geochemistry and Ranging (MESSENGER) data, the viscoelastic component remains to be determined.

Theory: The tidal potential W is determined by the mass of the central body, the radius of the body as well as the orbital and rotational characteristics and is given by

$$W(r,\phi) = \frac{GM}{r'}\sum_{l=2}^{\infty}\left(\frac{r}{r'}\right)^{l} P_{l0}(\cos\phi)\,, \qquad (1)$$

where G is the gravitational constant, M is the mass of the tide generating body, r' is the distance between the two bodies, $P_{l0}(\cos\phi)$ are the associated Legendre polynomials of degree l and order 0, ϕ is the body-centered angle between the central body at the point selected for the potential and r is the distance to the center of mass of the body at that point. Hence, the time-dependent properties of the tidal potential are determined by r' and ϕ. As with increasing order l the tidal potential declines with $1/r'^{l+1}$ $t$he expansion is limited to the second degree, i.e. $l = 2$,

$$W_2(r,\phi) = \frac{GMr^2}{r'^3}P_{20}(\cos\phi)\,, \qquad (2)$$

with $P_{20}(x) = (3x^2-1)/2$. Following the formalism in [1] we can use spherical harmonic functions $Y_m^l(\theta,\lambda)$ and time-dependent distortion coefficients $C_{lm}(t)$ and $S_{lm}(t)$ to transform this expression to

$$W_2(r,\theta,\lambda,t) = \frac{GMr^2}{a^3}\sum_{m=0}^{2} Y_m^2(\theta,\lambda)C_{2m}(t) + Y_{-m}^2(\theta,\lambda)S_{2m}(t), \qquad (3)$$

where r,θ,λ are spherical coordinates (radius, latitude, longitude) of the point of interest and t is the time. a is the semi-major axis and is only introduced to scale the coefficients C_{2m} and S_{2m}. It is convenient to expand the distortion coefficients $C_{lm}(t)$ and $S_{lm}(t)$ in a time series

$$\begin{matrix} C_{2m}(t) \\ S_{2m}(t) \end{matrix} = \begin{matrix} C_{2m}^* \\ S_{2m}^* \end{matrix} + \sum_{i=0}^{\infty} \begin{matrix} C_{2m}^{(i)} \cos \\ S_{2m}^{(i)} \sin \end{matrix}(\omega_i t + \varphi_i)\,, \qquad (4)$$

where C_{2m}^* and S_{2m}^* denote the static components of the tidal potential and $C_{2m}^{(i)}$ and $S_{2m}^{(i)}$ are the amplitudes associated with frequency ω_i and phase φ_i. For a Keplerian orbit of Mercury with eccentricity e (in first order) and mean anomaly M the term $C_{20}(t)$ takes the form [2]

$$\begin{aligned} C_{20}(t) &= C_{20}^* + C_{2m}^{(0)}\cos(\omega_0 t + \varphi_0) \qquad (5)\\ &= -\frac{1}{2} - \frac{3}{2}e\,\cos M + O(e^2). \end{aligned}$$

As the orbit may feature significant perturbations and the rotation state might include libration and precession the simplifications made in Eq. 5 may not provide a comprehensive description of the tidal potential. Better results are obtained by performing a frequency decomposition of the time series for $C_{2m}(t)$ and $S_{2m}(t)$.

The response of a body to the tidal potential is typically described by Love-Shida numbers k, h and l. For the degree-two tidal potential, k_2 describes the variation of the gravity field, while h_2 and l_2 describe the radial and lateral deformation of the surface, respectively. In case of an elastic response the potential V due the tidal distortion of the body takes the form

$$\begin{aligned} V_2(r,\theta,\lambda,t) = \frac{GMr^2}{a^3} \qquad (6)\\ k_2^f \sum_{m=0}^{2} C_{2m}^* Y_m^2(\theta,\lambda) + S_{2m}^* Y_{-m}^2(\theta,\lambda) + \\ \sum_{i=0}^{\infty}\sum_{m=0}^{2} k_2^{(i)} C_{2m}^{(i)} Y_m^2(\theta,\lambda)\cos(\omega_i t + \varphi_i) + \\ k_2^{(i)} S_{2m}^{(i)} Y_{-m}^2(\theta,\lambda)\sin(\omega_i t + \varphi_i), \end{aligned}$$

where $k_2^{(i)}$ are the degree-two frequency-dependent elastic Love numbers and k_2^f is the degree-two fluid Love number. We do not recall the equation for a viscoelastic response and refer the reader to equations provided in [1].

MESSENGER observations: Most recent measurements of Mercury's k_2 suggest values between 0.569 ± 0.025 [3] and 0.53 ± 0.03 [4]. For the radial deformation of the surface a value of $h_2 = 1.55 \pm 0.65$ [5] was estimated. All these estimates neglected the frequency dependence of the tidal response, i.e. $k_2 = k_2^{(i)}$ and $h_2 = h_2^{(i)}$. Viscoelastic deformation was

so far not measured for Mercury. However, modelling suggests phase-lags for k_2 and h_2 of up to 4°, i.e. about 1 day [6]. Accurate measurements of the phase-lags may lead to tight constraints of the rheological parameters of Mercury's mantle and inner core.

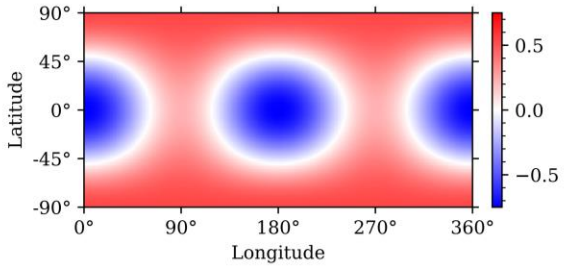

Fig. 1: Static part of Mercury's tidal potential.

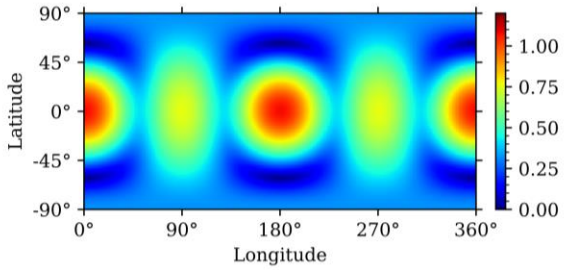

Fig. 2: Tidal potential amplitudes at the surface of Mercury for the 87.969 days component.

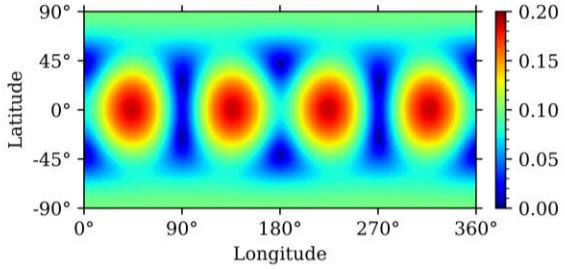

Fig. 3: Tidal potential amplitudes at the surface of Mercury for the 43.985 days component.

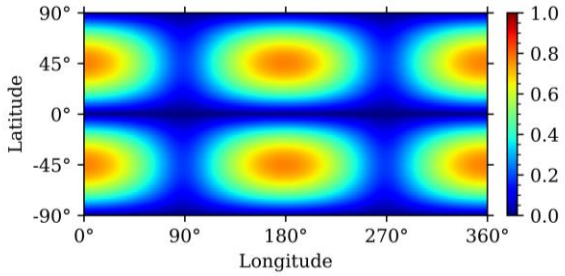

Fig. 4: Tidal potential amplitudes (scaled by 10^3) at the surface of Mercury for the 58.6462 days component.

Frequency-dependent tidal potential: For our analysis we used INPOP19a ephemerides [7] and Mercury's rotation state as given in the IAU report 2015 [8]. The tidal potential was computed using Eq. 2 on a global grid in time steps of 1.5 days. Each instantaneous tidal potential grid was then expanded in spherical harmonics leading to a time series for the distortion coefficients $C_{20}, C_{21}, C_{22}, S_{21}$ and S_{22}. For the zonal and sectorial coefficients, the dominating tidal periods are integer fractions of the orbital period 87.969/n days, i.e. 87.969 days, 43.985 days, 29.323 days and so on. For the tesseral coefficients, which are describing obliquity tides, we find integer fractions of the synodic day 175.9386/(2n+1) days, i.e. 175.9386 days, 58.6462 days, 35.1877 days and so on.

Fig. 1 shows the static part of Mercury's tidal potential. The dynamic part of the tidal potential is dominated by the 87.969 days component (Fig. 2). The maximal deformation is found at the "hot poles" of Mercury. Assuming a plausible value for the h_2 Love number of $h_2 = 0.85$ the peak-to-peak radial deformation at the surface would be at about 2.4 m. For the 43.985 days component of the tidal potential the amplitudes are significantly smaller, only 17% of the main component at 87.969 days (Fig. 3).

Obliquity tides of Mercury are very weak, less than 0.07% of the eccentricity tides (Fig. 4). Again, assuming $h_2 = 0.85$ the peak-to-peak deformation would be at most 17 cm for the 58.6462 days component.

The obtained results for the components of the tidal potential are consistent with earlier results [8]. Further work will investigate the viscoelastic response of Mercury to the different frequencies found in the analysis of the tidal potential.

Acknowledgements: This work has been funded by the French National Research Agency (ANR) and by the German Research Foundation (DFG) joined project ANR-19-CE31-0026.

References:

[1] Williams, J. G., Boggs, D. H. (2015). *JGR-Planets*, doi:10.1002/2014JE004755 **[2]** Steinbrügge, G. (2018). *PhD thesis*. Technische Universität Berlin, doi: 10.14279/depositonce-7118 **[3]** Genova, A., et al. (2019). *GRL*, doi: 10.1029/2018GL081135 **[4]** Konopliv, A. et al (2020). *Icarus*. doi: 10.1016/j.icarus.2019.07.020 **[5]** Bertone, S., et al. (2021). *JGR-Planets*, doi:10.1029/ 2020JE006683 **[6]** Steinbrügge, G., et al. (2018). *JGR-Planets*, doi:10.1029/2018je005569 **[7]** Fienga, A., et al. (2019). ISBN 978-2-910015-81-7 **[8]** Archinal, B. A., et al. (2018), *CMDA*, doi:10.1007/s10569-017-9805-5 **[8]** Van Hoolst, T, Jacobs, C. (2003). *JGR-Planets,* doi:10.1029/2003je002126